
Bootstrapping Neural Processes

**Juho Lee^{1,2*}, Yoonho Lee^{2*}, Jungtaek Kim³,
Eunho Yang^{1,2}, Sung Ju Hwang^{1,2}, Yee Whye Teh⁴**
KAIST¹, Daejeon, South Korea, AITRICS², Seoul, South Korea,
POSTECH³, Pohang, South Korea, University of Oxford⁴, Oxford, England
juholee@kaist.ac.kr

Abstract

Unlike in the traditional statistical modeling for which a user typically hand-specify a prior, Neural Processes (NPs) implicitly define a broad class of stochastic processes with neural networks. Given a data stream, NP learns a stochastic process that best describes the data. While this “data-driven” way of learning stochastic processes has proven to handle various types of data, NPs still rely on an assumption that uncertainty in stochastic processes is modeled by a single latent variable, which potentially limits the flexibility. To this end, we propose the Bootstrapping Neural Process (BNP), a novel extension of the NP family using the bootstrap. The bootstrap is a classical data-driven technique for estimating uncertainty, which allows BNP to learn the stochasticity in NPs without assuming a particular form. We demonstrate the efficacy of BNP on various types of data and its robustness in the presence of model-data mismatch.

1 Introduction

Neural Process (NP) [10] is a class of stochastic processes defined by parametric neural networks. Traditional stochastic processes such as Gaussian Process (GP) [25] are usually derived from mathematical objects based on certain prior beliefs on data (e.g., smoothness of functions quantified by Gaussian distributions). On the other hand, given a stream of data, NP *learns* to construct a stochastic process that might describe the data well. In that sense, NP may be considered as a data-driven way of defining stochastic processes. When appropriately trained, NP can define a flexible class of stochastic processes well suited for highly non-trivial functions that are not easily represented by existing stochastic processes.

Like other stochastic processes, NP induces stochasticity in function realizations. More specifically, NP defines a function value y for a point x as a conditional distribution $p(y|x, \dots)$ to model *point-wise uncertainty*. Additionally, NP further introduces a *global latent variable* capturing *functional uncertainty* - a global uncertainty in the overall structure of the function. The global latent variable modeling functional uncertainty is empirically demonstrated to improve the predictive performance and diversity in function realizations [20].

Although it is clear both intuitively and empirically that adding functional uncertainty helps, it remains unclear whether modeling it with a single Gaussian latent variable is optimal. For instance, [22] pointed out that the global latent variable acts as a bottleneck. One could introduce more complex architectures to better capture the functional uncertainty, but that would typically come with an architectural overhead. Moreover, it contradicts the philosophy behind NP to use minimal modeling assumptions and let the model learn from data.

* Equal contribution

This paper introduces a novel way of introducing functional uncertainty to the family of NP models. We revisit the bootstrap [8], a classic frequentist technique to model uncertainty in parameter estimation by simulating population distribution via resampling. The bootstrap is a simple yet effective way of modelling uncertainty in a data-driven way, making it well-suited for our purpose of giving uncertainty to NP with minimal modeling assumptions. To this end, we propose BNP, an extension of NP using bootstrap to induce functional uncertainty. BNP utilizes bootstrap to construct multiple resampled datasets and combines the predictions computed from them. The functional uncertainty is then naturally induced by the uncertainty in the bootstrap procedure.

BNP can be defined for any existing NP variants with minimal additional parameters and provides several benefits over existing models. One important aspect is its robustness under the presence of *model-data mismatch*, where test data come from distributions different from the one used to train the model. An ensemble of bootstrap is well known to enhance the stability and accuracy [2]. Recently, [13] showed that ensembling Bayesian posteriors from multiple bootstrap samples dramatically improves the robustness under model-data mismatch. We show that our extension of NP with bootstrap also enjoys this property. Using various data ranging from simple synthetic data to challenging real-world data, we demonstrate that BNP is much more robust than the existing NP with global latent variables. This tendency was particularly strong under model-data mismatch, where the test data is significantly different from the datasets used to train the model.

2 Background

2.1 (Attentive) Neural Processes

Consider a regression task $\mathcal{T} = (X, Y, c)$ defined by an observation set $X = \{x_i\}_{i=1}^n$, a label set $Y = \{y_i\}_{i=1}^n$, and an index set $c \subsetneq \{1, \dots, n\}$ defining *context* $(X_c, Y_c) := \{(x_i, y_i)\}_{i \in c}$. The goal is to learn a stochastic process (random function) mapping x to y given the context (X_c, Y_c) as training data (a realization from the stochastic process), i.e., learning

$$\log p(Y|X, Y_c) = \sum_{i=1}^n \log p(y_i|x_i, X_c, Y_c). \quad (1)$$

Conditional Neural Process (CNP) [9] models $p(y_i|x_i, X_c, Y_c)$ with a deterministic neural network taking (X_c, Y_c) and x_i to output the parameters of $p(y_i|x_i, X_c, Y_c)$. CNP consists of an encoder and a decoder; the encoder summarizes (X_c, Y_c) into a representation ϕ via permutation-invariant neural network [7, 31], and the decoder transforms ϕ and x_i into the target distribution (e.g., Gaussian),

$$\phi = f_{\text{enc}}(X_c, Y_c) = f_{\text{enc}}^{(2)}\left(\frac{1}{|c|} \sum_{i \in c} f_{\text{enc}}^{(1)}(x_i, y_i)\right), \quad (2)$$

$$(\mu_i, \sigma_i) = f_{\text{dec}}(\phi, x_i), \quad p(y_i|x_i, X_c, Y_c) = \mathcal{N}(y_i|\mu_i, \sigma_i^2), \quad (3)$$

where $f_{\text{enc}}^{(1)}$, $f_{\text{enc}}^{(2)}$ and f_{dec} are feed-forward neural networks. CNP is then trained to maximize the expected likelihood $\mathbb{E}_{p(\mathcal{T})}[\log p(Y|X, Y_c)]$. The variance σ_i^2 models the *point-wise* uncertainty for y_i given the context. NP [10] further models *functional uncertainty* using a *global latent variable*. Unlike CNP, which maps a context into a deterministic representation ϕ , NP encodes the context into a Gaussian latent variable z , giving additional stochasticity in function construction. Following [15], we consider a NP with both deterministic path and latent path, where the deterministic path models the overall skeleton of the function ϕ , and the latent path models the functional uncertainty:

$$\phi = f_{\text{denc}}(X_c, Y_c), \quad (\eta, \rho) = f_{\text{enc}}(X_c, Y_c), \quad q(z|X_c, Y_c) = \mathcal{N}(z; \eta, \rho^2) \quad (4)$$

$$(\mu_i, \sigma_i) = f_{\text{dec}}(\phi, z, x_i), \quad p(y_i|x_i, z, \phi) = \mathcal{N}(y_i|\mu_i, \sigma_i^2), \quad (5)$$

with f_{denc} and f_{enc} having the same structure as f_{enc} in (2). The conditional probability is lower-bounded as

$$\log p(Y|X, Y_c) \geq \sum_{i=1}^n \mathbb{E}_{q(z|X, Y)} \left[\log \frac{p(y_i|x_i, z, \phi)p(z|X_c, Y_c)}{q(z|X, Y)} \right]. \quad (6)$$

We further approximate $p(z|X_c, Y_c) \approx q(z|X_c, Y_c)$ and train the model by maximizing this expected lower-bound over tasks.

Attentive Neural Process (ANP) [15] and its conditional version without a global latent variable, Conditional Attentive Neural Process (CANP), both employ an attention mechanism [28] to resolve the issue of underfitting in the vanilla NP model. The encoder in ANP utilizes self-attention and cross-attention operation to better summarize the context into a representation ϕ . Please refer to [Appendix A](#) for a detailed description about the architectures.

2.2 Bootstrap, Bagging, and BayesBag

Let $X = \{x_i\}_{i=1}^n$ be a dataset and $\theta = F(X)$ a parameter to estimate. Bootstrap [8] is a method that estimates the sampling distribution of θ from multiple datasets resampled from X ,

$$\tilde{X}^{(j)} \stackrel{\text{s.w.r.}}{\sim} X, \quad \tilde{\theta}^{(j)} = F(\tilde{X}^{(j)}) \quad \text{for } j = 1, \dots, k, \quad (7)$$

where $\stackrel{\text{s.w.r.}}{\sim}$ denotes sampling with replacement ¹. We call each $\tilde{X}^{(j)}$ a *bootstrap dataset* and $\tilde{\theta}^{(j)}$ a *bootstrap estimate*. The bootstrap estimates are used for assessing uncertainty, computing credible intervals, or statistical testing. One can interpret the bootstrap estimates as samples from an (approximate) nonparametric and noninformative posterior of θ [12, page 272]. Contrary to standard Bayesian methods that specify an explicit prior $p(\theta)$, bootstrapping is a more “data-driven” way of computing the uncertainty of θ .

Bootstrap aggregating (bagging) [2] is a procedure that ensembles multiple predictors given by bootstrap estimates. Let $T(\theta)$ be a predictor based on a parameter θ , and $\{\tilde{\theta}^{(j)}\}_{j=1}^k$ be bootstrap estimates. The bagging predictor is computed as $\frac{1}{k} \sum_{j=1}^k T(\tilde{\theta}^{(j)})$. Bagging is known to improve accuracy and stability on classification and regression problems [2].

Instead of point estimates $T(\theta)$, one can also apply bagging to *Bayesian posteriors* $p(T(\theta)|X)$. BayesBag [6, 13] ensembles posteriors $\{p(T(\theta)|\tilde{X}^{(j)})\}_{j=1}^k$ computed from bootstrapped datasets to get an aggregated posterior $\frac{1}{k} \sum_{j=1}^k p(T(\theta)|\tilde{X}^{(k)})$. Compared to bagging, BayesBag provides similar or often better results even with fewer bootstrap datasets and is more robust under model-data mismatch [13].

2.3 Residual Bootstrap

Consider the bootstrap for regression, where a dataset is $(X, Y) = \{(x_i, y_i)\}_{i=1}^n$ and we want to estimate the distribution of the regression parameters θ or the predictive distribution $p(y|x, \theta)$. The most straightforward way is the paired bootstrap (empirical bootstrap) where we resample pairs of (x, y) with replacement: $\{(\tilde{x}_i, \tilde{y}_i)\}_{i=1}^n \stackrel{\text{s.w.r.}}{\sim} \{(x_i, y_i)\}_{i=1}^n$. Unfortunately, since the probability of a pair (x_i, y_i) being excluded in (\tilde{X}, \tilde{Y}) is approximately $(1 - n^{-1})^n \xrightarrow{n \rightarrow \infty} 0.368$, influential observations are often discarded, degrading the predictive accuracy.

Another option is the *residual bootstrap* which fixes X and only resamples the residuals of predictions. Consider a nonparametric regression setting with prediction μ_i , variance σ_i^2 , and additive residual ε_i (μ_i and σ_i are functions of x_i), i.e., $y_i = \mu_i + \sigma_i \varepsilon_i$. Then, the bootstrap datasets are resampled as

1. Fit a model with (X, Y) to obtain $\{(\mu_i, \sigma_i)\}_{i=1}^n$ and compute the residual $\varepsilon_i = \frac{y_i - \mu_i}{\sigma_i}$.
2. Let $\mathcal{E} = \{\varepsilon_i\}_{i=1}^n$, For $j = 1, \dots, k$,
 - (a) Resample the residuals: $\tilde{\varepsilon}_1^{(j)}, \dots, \tilde{\varepsilon}_n^{(j)} \stackrel{\text{s.w.r.}}{\sim} \mathcal{E}$.
 - (b) Construct a bootstrap dataset: for $i = 1, \dots, n$, $\tilde{x}_i^{(j)} = x_i$, $\tilde{y}_i^{(j)} = \mu_i + \sigma_i \tilde{\varepsilon}_i^{(j)}$.

The residual bootstrap resolves the issue of missing x in bootstrap datasets, which is why they are often recommended for regression problems. We focus on using the residual bootstrap for our purpose, but one may also consider alternative bootstrap variants (e.g., wild bootstrap, parametric bootstrap) to resample datasets.

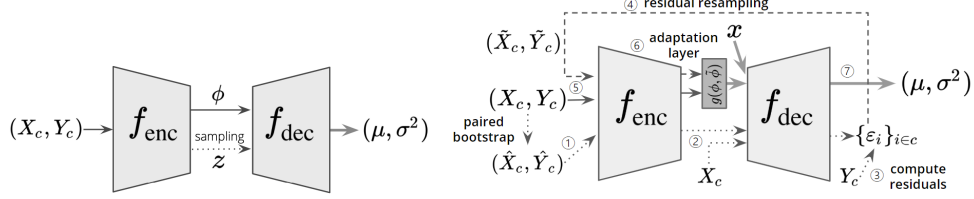


Figure 1: Diagrams for NP (left) and BNP (right).

3 Bootstrapping Neural Processes

3.1 Naïve application of residual bootstrap to NP does not work

One may consider directly applying residual bootstrap to existing NP models. That is, given a task $\mathcal{T} = (X, Y, c)$ and a NP model trained ordinarily, we can directly apply the residual bootstrap procedure described in Section 2.3 to get bootstrap contexts, and then compute bagged predictions by forwarding the bootstrap contexts through the NP model. NP is especially well-suited to this procedure because of its *amortization* in the inference step – it computes conditional probability $p(y|x, X_c, Y_c)$ efficiently as forward passes through neural networks. However, unfortunately, we found this works poorly in terms of predictive accuracy (Table D.5). This may be because 1) the amortization is suboptimal, making the errors from fitting multiple bootstrap datasets accumulate, and 2) the NP model does not see bootstrap datasets during training, so feeding bootstrap datasets through the network acts like a model-data mismatch scenario that can fool the model.

3.2 Bootstrapping Neural Processes

Beyond naïvely applying bootstrap to NP, we propose a novel class of NP called Bootstrapping Neural Process (BNP) which explicitly uses bootstrap datasets as additional inputs to induce functional uncertainty. BNP uses the NP as its “base” model, and the extension to ANP which we name Bootstrapping Attentive Neural Process (BANP) is defined similarly. Let f_{enc} and f_{dec} be encoder and decoder of a base NP (defined as in (2)), and $\mathcal{T} = (X, Y, c)$ be a task. BNP computes predictions through the following steps.

Resampling contexts via paired bootstrap Before proceeding to residual bootstrap, we first resample the contexts from (X_c, Y_c) via paired bootstrap, that is, for $j = 1, \dots, k$,

$$(\hat{X}_c^{(j)}, \hat{Y}_c^{(j)}) := \{(\hat{x}_i^{(j)}, \hat{y}_i^{(j)})\}_{i=1}^{|c|} \stackrel{\text{s.w.r.}}{\sim} \{(x_i, y_i)\}_{i \in c}. \quad (8)$$

As noted in Section 2.3, some resampled context $(\hat{X}_c^{(j)}, \hat{Y}_c^{(j)})$ may miss several pairs from the original context. When passed to the model, such context would produce bad predictors, and thus large residuals. We empirically found that instead of computing single residuals computed from the full context (X_c, Y_c) as in ordinary residual bootstrap, computing residuals from the multiple resampled contexts enhances robustness by exposing the model to residuals with diverse patterns during training. We present an ablation study comparing BNP with and without this step in Table D.5.

Residual bootstrap Now we do the inference for the full context (X_c, Y_c) using the resampled contexts $(\hat{X}_c^{(j)}, \hat{Y}_c^{(j)})$. As noted above, this can be done efficiently by forwarding $(\hat{X}_c^{(j)}, \hat{Y}_c^{(j)})$ through $f_{\text{enc}}, f_{\text{dec}}$ to get $\{(\hat{\mu}_i, \hat{\sigma}_i)\}_{i \in c}$.

$$\hat{\phi}^{(j)} = f_{\text{enc}}(\hat{X}_c^{(j)}, \hat{Y}_c^{(j)}), \quad (\hat{\mu}_i^{(j)}, \hat{\sigma}_i^{(j)}) = f_{\text{dec}}(x_i, \hat{\phi}^{(j)}) \text{ for } i \in c. \quad (9)$$

Following the residual bootstrap procedure, we first compute residual, resample them,

$$\varepsilon_i^{(j)} = \frac{y_i - \hat{\mu}_i^{(j)}}{\hat{\sigma}_i^{(j)}} \text{ for } i \in c, \quad \mathcal{E}^{(j)} = \{\varepsilon_i^{(j)}\}_{i=1}^c, \quad \tilde{\varepsilon}_1^{(j)}, \dots, \tilde{\varepsilon}_{|c|}^{(j)} \stackrel{\text{s.w.r.}}{\sim} \mathcal{E}^{(j)}. \quad (10)$$

and construct bootstrap contexts to be used for the final prediction.

$$\begin{aligned} \tilde{x}_i^{(j)} &= x_i, \quad \tilde{y}_i^{(j)} = \hat{\mu}_i^{(j)} + \hat{\sigma}_i^{(j)} \tilde{\varepsilon}_i^{(j)} \text{ for } i \in c, \\ (\tilde{X}_c^{(j)}, \tilde{Y}_c^{(j)}) &:= \{(\tilde{x}_i^{(j)}, \tilde{y}_i^{(j)})\}_{i \in c} \text{ for } j = 1, \dots, k. \end{aligned} \quad (11)$$

¹Unless specified otherwise, we sample the same number of elements as the original set: $|X| = |\tilde{X}^{(j)}|$.

Encoding with adaptation layer We pass the bootstrap contexts into the encoder to get the representations of the contexts, $\tilde{\phi}^{(j)} = f_{\text{enc}}(\tilde{X}_c^{(j)}, \tilde{Y}_c^{(j)})$ for $j = 1, \dots, k$. The ordinary residual bootstrap would put each $\tilde{\phi}^{(j)}$ into the decoder and ensemble the decoded conditional probabilities. Instead, like NP using both deterministic representation ϕ and global latent variable z , we put both the representation of the original context $\phi = f_{\text{enc}}(X_c, Y_c)$ and the bootstrapped representation $\tilde{\phi}^{(j)}$ into the decoder. Since the decoder f_{dec} is built to take only ϕ , we add an *adaptation layer* $g(\phi, \tilde{\phi}^{(j)})$ to let f_{dec} process a combined representation. The adaptation layer is the only part that we add to the base model, and can be implemented with a single linear layer. We empirically demonstrated that the adaptation layer is crucial for accurate prediction (Table D.5).

Prediction Finally, we construct predictions by ensembling the predictions decoded from the representations of bootstrap contexts. For a target point x_i ,

$$(\mu_i^{(j)}, \sigma_i^{(j)}) = f_{\text{dec}}(g(\phi, \tilde{\phi}^{(j)}), x_i), \quad p(y_i|x_i, \phi, \tilde{\phi}^{(j)}) = \mathcal{N}(y_i|\mu_i^{(j)}, (\sigma_i^{(j)})^2). \quad (12)$$

We compute this for $j = 1, \dots, k$ to get an ensembled distribution,

$$p(y_i|x_i, X_c, Y_c) \approx \frac{1}{k} \sum_{j=1}^k \mathcal{N}(y_i|\mu_i^{(j)}, (\sigma_i^{(j)})^2). \quad (13)$$

Fig. 1 shows diagrams comparing NP and BNP. BNP uses almost the same architecture except for the adaptation layer, but goes through the encoding-decoding process twice (first to compute residuals only using the base model, and second to compute prediction with the adaptation layer added).

3.3 Training

BNP requires special care for training because we need to balance the training of the base model (without bootstrap) and the full model (with bootstrap). If we only train the full model, the decoder of the base model computing the residuals would produce inaccurate predictions yielding large residuals, making the full model likely to ignore the residual path during the early training stages. To resolve this, we train the model with a combined objective to simultaneously train two paths as follows,

$$\mathbb{E}_{p(\mathcal{T})} \left[\sum_{i=1}^n \left(\log p_{\text{base}}(y_i|x_i, X_c, Y_c) + \log \frac{1}{k} \sum_{j=1}^k \mathcal{N}(y_i|\mu_i^{(j)}, (\sigma_i^{(j)})^2) \right) \right], \quad (14)$$

where $p_{\text{base}}(y_i|x_i, X_c, Y_c)$ denotes the conditional probability computed from the base model (see Table D.5 for the ablation study). We also found that training with multiple bootstrap contexts (13) ($k > 1$) is crucial for robustness. We fixed $k = 4$ for all of our experiments.

3.4 Discussion

Parallel computation An advantage of bootstrap and bagging is the ease in parallelization of fitting multiple bootstrap datasets. Our model also enjoys such benefits: we compute all steps (8)-(11) in parallel by packing multiple bootstrap contexts into a tensor and feeding it through networks.

Our model and BayesBag Note that we are computing the aggregated conditional probability (13), which is similar to how BayesBag computes the aggregated posterior. The difference is that we aggregate the approximate distributions computed with a shared neural network (f_{enc} and f_{dec}) while BayesBag independently computes posteriors. Although the theory in [13] does not directly apply to BNP, the underlying intuition may still be valid for our model: the predictions computed from BayesBag is more conservative (and thus robust) because it combines the model’s uncertainty with the data-driven uncertainty coming from bootstrap.

Why should NP be robust? Although we do not have theoretical claims that explain our model’s robustness, we have intuitive explanations for such properties. When a BNP model encounters a substantial shift in data distribution, the base model will fail, resulting in larger residuals than usual. These larger residuals will be reflected in bootstrap contexts and thus into the representations $\tilde{\phi}^{(j)}$. This encourages the model to produce more conservative (larger σ_i^2) results (e.g, Fig. 2).

Table 1: 1D regression results. “context” refers to context log-likelihoods, and “target” refers to target log-likelihoods. Means and standard deviations of five runs are reported.

	RBF		Matérn 5/2		Periodic		t -noise	
	context	target	context	target	context	target	context	target
CNP	0.972 \pm 0.008	0.448 \pm 0.006	0.846 \pm 0.009	0.206 \pm 0.006	-0.163 \pm 0.008	-1.747 \pm 0.023	0.363 \pm 0.147	-1.528 \pm 0.068
NP	0.902 \pm 0.009	0.420 \pm 0.008	0.774 \pm 0.012	0.204 \pm 0.010	-0.181 \pm 0.010	-1.338 \pm 0.025	0.442 \pm 0.016	-0.792 \pm 0.048
CNP+DE	0.995	0.521	0.878	0.313	-0.098	-1.384	0.534	-1.129
BNP	1.013 \pm 0.007	0.526 \pm 0.005	0.890 \pm 0.009	0.317 \pm 0.006	-0.112 \pm 0.007	-1.082 \pm 0.011	0.553 \pm 0.009	-0.630 \pm 0.014
CANP	1.379 \pm 0.000	0.838 \pm 0.001	1.376 \pm 0.000	0.652 \pm 0.001	0.476 \pm 0.043	-5.896 \pm 0.134	1.104 \pm 0.009	-2.243 \pm 0.031
ANP	1.379 \pm 0.000	0.842 \pm 0.002	1.376 \pm 0.000	0.660 \pm 0.001	0.600 \pm 0.034	-4.357 \pm 0.182	1.125 \pm 0.003	-1.776 \pm 0.021
CANP+DE	1.378	0.847	1.376	0.670	0.771	-4.598	1.161	-1.991
BANP	1.379 \pm 0.000	0.851 \pm 0.002	1.376 \pm 0.000	0.672 \pm 0.001	0.705 \pm 0.016	-3.275 \pm 0.114	1.142 \pm 0.007	-1.718 \pm 0.055

4 Related Works

Since the first model CNP [9], there have been several follow-up works to improve NP classes in various aspects. NP [10] suggested to use a global latent variable to model functional uncertainty. ANP [15] further improved the reconstruction quality by employing attention mechanism, and [20] conducted comprehensive comparison and empirically concluded that having global latent variable helps. [27, 30] extended NP to work for sequential data. [22] proposed a consistent NP model mainly using graph neural networks to build conditional probabilities. [11] proposed a translation-equivariant version of NP model using convolution operation in context encoding.

Bootstrap and bagging have been used ubiquitously over many areas in statistical modeling and machine learning. We list a few recent works (especially in the deep learning era) that have benefited from bootstrap and related ideas. Deep ensemble [19] is a special case of bagging (but resampling with replacement) and has been shown to improve predictive accuracy and robustness on various tasks. [26] demonstrated that bootstrapping can improve classification performance on noisy or incomplete labels. [24] showed that bootstrapping can improve exploration in deep reinforcement learning. [23], which proposed the amortized bootstrap, is probably the most similar work to ours. They learn an implicit distribution that generates bootstrap estimates of a parameter of interest, and they show that bagging the bootstrap estimates generated from learned distribution outperforms ordinary bagging. The difference is that the amortized bootstrap targets a single task, meaning that they only learn an implicit bootstrap distribution for a single dataset. On the other hand, BNP meta-learns a network that performs bootstrapping and bagging for any dataset from a particular task distribution.

5 Experiments

In this section, we compare the baseline NP classes (CNP, NP, CANP, and ANP) to our models (BNP, BANP) on both synthetic and real-world datasets. We also compare ours against Deep Ensemble (DE) of CNP and CANP [19], in which five identical models are trained with different random initializations and data streams, and averaged for prediction.² Following [15], we measured the *context likelihood* $\frac{1}{|c|} \sum_{i \in c} \log p(y_i | x_i, X_c, Y_c)$ measuring the reconstruction quality of the contexts and *target likelihood* $\frac{1}{n-|c|} \sum_{i \notin c} \log p(y_i | x_i, X_c, Y_c)$ measuring the prediction accuracy. NP, ANP, BNP, and BANP were trained with $k = 4$ samples (z for NP and ANP, and bootstrap contexts for BNP and BANP) and tested with $k = 50$ samples. Please refer to Appendix B for further details.

5.1 1D Regression

We first conducted 1D regression experiments as in [15]. We trained the models with curves generated from GP with RBF kernels and tested in various settings, including model-data mismatch. More specifically, we tested the models trained with RBF kernel on the data generated from GP with other

²One could also consider DE of NP or BNP, but here we want to compare the net effect of DE without any other source of uncertainty.

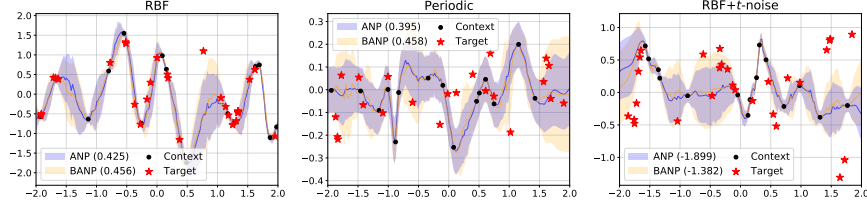


Figure 2: Visualization of ANP and BANP for 1D regression data. Ensembled means and \pm standard deviations of 50 samples are displayed. The numbers in the legend denotes target log-likelihoods.

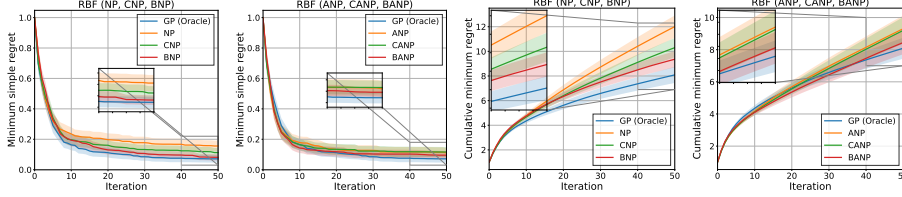


Figure 3: Bayesian optimization results for GP prior functions with RBF.

types of kernels (Matérn 5/2, Periodic), and GP with Student’s t noise added (t -noise). Please refer to [Appendix B.1](#) for a detailed description of network architectures, data generation, training, and testing. For a fair comparison, we set the models to use almost the same number of parameters. [Table 1](#) summarizes the results. BNP and BANP outperformed baselines and even DE, which has $5\times$ the number of parameters. As expected, all models are less accurate in the model-data mismatch setting, but BNP and BANP were affected less, demonstrating the robustness of our approach. [Fig. 2](#) illustrates the behaviour of BANP: ANP and BANP show similar variances for ordinary test data (RBF), but for model-data mismatch data (periodic and t -noise), BANP produces wider variances than ANP. We further analyze this aspect by looking at calibrations and sharpness of the predictions in [Appendix C](#).

5.2 Bayesian Optimization

We evaluated the models trained in [Section 5.1](#) on Bayesian optimization [3] for functions generated from a GP prior. We reported the best simple regret, which represents the difference between the current best observation and the global optimum, and the cumulative best simple regret for 100 sampled functions. For consistent comparison, we fixed initializations and normalized the results. Results in [Fig. 3](#) show that BNP and BANP consistently achieve lower regret than other NP variants. See [Appendix B.2](#) for more results including model-data mismatch settings.

Table 2: EMNIST results. Means and standard deviations of 5 runs are reported.

	Seen classes (0-9)		Unseen classes (10-46)		t -noise	
	context	target	context	target	context	target
CNP	0.926 ± 0.007	0.751 ± 0.005	0.766 ± 0.009	0.498 ± 0.012	-0.288 ± 0.140	-0.478 ± 0.129
NP	0.948 ± 0.006	0.806 ± 0.005	0.808 ± 0.005	0.600 ± 0.009	0.071 ± 0.042	-0.146 ± 0.034
CNP+DE	0.954	0.813	0.818	0.616	0.107	-0.020
BNP	1.004 ± 0.008	0.880 ± 0.005	0.883 ± 0.010	0.722 ± 0.006	-0.027 ± 0.069	0.003 ± 0.037
CANP	1.383 ± 0.000	0.950 ± 0.004	1.382 ± 0.000	0.834 ± 0.002	0.133 ± 0.196	-0.492 ± 0.108
ANP	1.383 ± 0.000	0.993 ± 0.005	1.383 ± 0.000	0.894 ± 0.004	0.249 ± 0.084	-0.132 ± 0.029
CANP+DE	1.383	0.976	1.383	0.881	0.307	-0.240
BANP	1.383 ± 0.000	1.010 ± 0.006	1.382 ± 0.000	0.942 ± 0.005	0.524 ± 0.102	0.124 ± 0.060

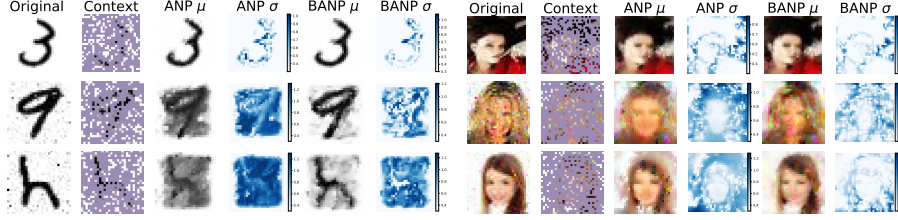


Figure 4: ANP vs BANP on EMNIST and CelebA32. The second and third row contains t -noises in the image. Ensembled means and standard deviations of 50 samples are displayed.

Table 3: CelebA32 results.

	Without noise		t -noise	
	context	target	context	target
CNP	2.975 ± 0.013	2.199 ± 0.003	0.350 ± 0.384	-1.468 ± 0.329
NP	3.066 ± 0.011	2.492 ± 0.014	0.005 ± 0.195	-0.217 ± 0.104
CNP+DE	3.082	2.426	1.361	-0.451
BNP	3.269 ± 0.008	2.788 ± 0.005	1.224 ± 0.422	0.454 ± 0.094
CANP	4.150 ± 0.000	2.731 ± 0.006	2.985 ± 0.149	-0.730 ± 0.045
ANP	4.150 ± 0.000	2.947 ± 0.007	3.037 ± 0.102	-0.099 ± 0.150
CANP+DE	4.150	2.814	3.401	-0.0466
BANP	4.149 ± 0.000	3.129 ± 0.005	3.395 ± 0.078	0.083 ± 0.126

Table 4: Predator-prey model results.

	Simulated		Real	
	context	target	context	target
CNP	0.088 ± 0.031	-0.142 ± 0.028	-2.702 ± 0.007	-3.013 ± 0.025
NP	-0.002 ± 0.039	-0.252 ± 0.036	-2.747 ± 0.019	-3.057 ± 0.020
CNP+DE	0.176	-0.026	-2.670	-2.952
BNP	0.213 ± 0.045	-0.011 ± 0.041	-2.654 ± 0.005	-2.942 ± 0.010
CANP	2.573 ± 0.014	1.819 ± 0.021	1.767 ± 0.089	-8.007 ± 0.538
ANP	2.582 ± 0.007	1.828 ± 0.007	1.720 ± 0.257	-7.809 ± 0.642
CANP+DE	2.591	1.874	2.021	-5.440
BANP	2.586 ± 0.009	1.855 ± 0.009	1.783 ± 0.156	-5.465 ± 0.278

5.3 Image Completion

We compared the models on image completion tasks on EMNIST [5] and CelebA [21] (resized to 32×32). We followed the setting in [10, 15]; see Appendix B.3 for details. As a model-data mismatch setting, we trained the models for EMNIST using the first 10 classes and tested on the remaining 37 classes. We also tested the setting for which Student’s t -noise were added to the pixel values. We summarize results in Table 2 and Table 3. Except for BNP for EMNIST with t -noise setting, ours outperformed the baselines. Fig. 4 compares the completion results of ANP and BANP. ANP often breaks down with noise, while BANP successfully recovers the shapes of objects in images with less blur.

5.4 Predator-Prey Model

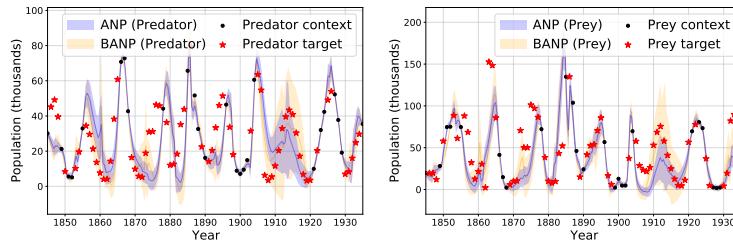


Figure 5: ANP vs BANP on Hudson’s Bay hare (right)-lynx (left) data. Ensembled means and standard deviations of 50 samples are displayed.

Finally, following [11], we applied the models to predator-prey population data. We first trained the models using simulated data generated from a Lotka-Volterra model [29] and tested on real-world data (Hudson’s Bay hare-lynx data). As noted and empirically demonstrated in [11], the hare-lynx data is quite different from the simulated data, so it acts as a mismatch scenario. The results are summarized in Table 4. We obtained the similar results as before; BNP and BANP outperformed the baselines and were comparable to DE for both simulated and real-world data. Fig. 5 shows a similar trend as in Fig. 2; BANP tends to be more conservative for mismatch data by producing larger variances.

6 Conclusion

In this paper, we proposed BNP, a novel member of the NP family, which uses bootstrapping to induce functional uncertainty. We demonstrated that BNP could successfully learn robust predictors, especially under model-data mismatch settings. Although not presented here, our model can be applied to any NP variants (or more) seamlessly. For instance, ours can readily be applied to recently proposed convolutional CNP [11]. As future work, one could consider developing a bootstrap resampling algorithm for more general settings. Here we presented an example of using residual bootstrap for regression, but this is not directly applicable for classification. Designing a framework that could “learn” to resample bootstrap datasets in a data-driven way would be an interesting and promising research direction. Finally, we want to stress that the idea of using bootstrap for inducing uncertainty may be useful for many other machine learning problems, especially the ones processing sets of data (e.g., [31]).

Broader Impact

Uncertainty, robustness, interpretability in predictions have been important desiderata for machine learning algorithms, especially because we have seen actual incidents showing that the algorithms without those could lead to serious damage even threatening human life. The proposed approach suggests a way to enhance robustness by considering uncertainty in data distribution, and the idea of enhancing robustness via bootstrap can be applied to many algorithms over various fields. Therefore, we think that our paper potentially has a positive impact on many areas. Among the experiments we conducted, the predator-prey data experiment (Section 5.4) shows this well, where data generated from a well-established model (Lotka-Volterra model) could be seriously different from real data (Hudson’s Bay hare-lynx data), and our model could reduce the risk of failure in such case. However, we admit that the proposed approach may still be vulnerable to various scenario could happen in real life, so should not be treated as an absolute standard to follow. Our model just reduces the probability of failure in a more natural way (i.e., more “data-driven” way).

Acknowledgments and Disclosure of Funding

This work was supported by Engineering Research Center Program through the National Research Foundation of Korea (NRF) funded by the Korean Government MSIT (NRF-2018R1A5A1059921), Institute of Information & communications Technology Planning & Evaluation (IITP) grant funded by the Korea government (MSIT) (No.2019-0-00075), IITP grant funded by the Korea government (MSIT) (No.2017-0-01779, XAI) and the grant funded by 2019 IT Promotion fund (Development of AI based Precision Medicine Emergency System) of the Korea government (Ministry of Science and ICT). EY is also supported by Samsung Advanced Institute of Technology (SAIT). YWT’s research leading to these results has received funding from the European Research Council under the European Union’s Seventh Framework Programme (FP7/2007-2013) ERC grant agreement no. 617071.

References

- [1] J. L. Ba, J. R. Kiros, and G. E. Hinton. Layer normalization. *arXiv preprint arXiv:1607.06450*, 2016.
- [2] L. Breiman. Bagging predictors. *Machine Learning*, 24(2):123–140, 1996.
- [3] E. Brochu, V. M. Cora, and N. de Freitas. A tutorial on Bayesian optimization of expensive cost functions, with application to active user modeling and hierarchical reinforcement learning. *arXiv preprint arXiv:1012.2599*, 2010.
- [4] Y. Burda, R. Grosse, and R. Salakhutdinov. Importance weighted autoencoders. In *International Conference on Learning Representations (ICLR)*, 2015.
- [5] G. Cohen, J. Afshar, S. adn Tapson, and A. van Schaik. EMNIST: an extension of MNIST to handwritten letters. *arXiv preprint arXiv:1702.05373*, 2017.

- [6] C. J. Douady, F. Delsuc, Y. Boucher, W. F. Doolittle, and D. E. J. P. Comparison of Bayesian and maximum likelihood bootstrap measures of phylogenetic reliability. *Molecular Biology and Evolution*, 20(2):248–254, 2003.
- [7] H. Edwards and A. Storkey. Towards a neural statistician. In *International Conference on Learning Representations (ICLR)*, 2016.
- [8] B. Efron. Bootstrap methods: another look at the jackknife. *Annals of Statistics*, 7(1):1–26, 1979.
- [9] M. Garnelo, D. Rosenbaum, C. J. Maddison, T. Ramalho, D. Saxton, M. Shanahan, Y. W. Teh, D. J. Rezende, and S. M. A. Eslami. Conditional neural processes. In *International Conference on Machine Learning (ICML)*, 2018.
- [10] M. Garnelo, J. Schwarz, D. Rosenbaum, F. Viola, D. J. Rezende, S. M. A. Eslami, and Y. W. Teh. Neural processes. *ICML Workshop on Theoretical Foundations and Applications of Deep Generative Models*, 2018.
- [11] J. Gordon, W. P. Bruinsma, A. Y. K. Foong, J. Requeima, Y. Dubois, and R. E. Turner. Convolutional conditional neural processes. In *International Conference on Learning Representations (ICLR)*, 2020.
- [12] T. Hastie, R. Tibshirani, and J. Friedman. *The Elements of Statistical Learning*. Springer Series in Statistics. Springer New York Inc., 2001.
- [13] J. H. Huggins and J. W. Miller. Using bagged posteriors for robust inference and model criticism. *arXiv preprint arXiv:1912.07104*, 2019.
- [14] D. R. Jones, M. Schonlau, and W. J. Welch. Efficient global optimization of expensive black-box functions. *Journal of Global Optimization*, 13:455–492, 1998.
- [15] H. Kim, A. Mnih, J. Schwarz, M. Garnelo, S. M. A. Eslami, D. Rosenbaum, and V. Oriol. Attentive neural processes. In *International Conference on Learning Representations (ICLR)*, 2018.
- [16] J. Kim and S. Choi. bayeso: A Bayesian optimization framework in Python. <http://bayeso.org>, 2017.
- [17] D. P. Kingma and J. Ba. Adam: a method for stochastic optimization. In *International Conference on Learning Representations (ICLR)*, 2015.
- [18] V. Kuleshov, N. Fenner, and S. Ermon. Accurate uncertainties for deep learning using calibrated regression. In *International Conference on Machine Learning (ICML)*, 2018.
- [19] B. Lakshminarayanan, A. Pritzel, and C. Blundell. Simple and scalable predictive uncertainty estimation using deep ensembles. In *Neural Information Processing Systems (NeurIPS)*, 2017.
- [20] T. A. Le, H. Kim, M. Garnelo, D. Rosenbaum, J. Schwarz, and Y. W. Teh. Empirical evaluation of neural process objectives. *NeurIPS Workshop on Bayesian Deep Learning*, 2018.
- [21] Z. Liu, P. Luo, X. Wang, and X. Tang. Deep learning face attributes in the wild. In *Proceedings of International Conference on Computer Vision (ICCV)*, 2015.
- [22] C. Louizos, X. Shi, K. Schutte, and M. Welling. The functional neural process. In *Neural Information Processing Systems (NeurIPS)*, 2019.
- [23] E. Nalisnick and P. Smyth. The amortized bootstrap. *ICML 2017 Workshop on Implicit Models*, 2017.
- [24] I. Osband, C. Blundell, A. Pritzel, and B. V. Roy. Deep exploration via bootstrapped DQN. In *Neural Information Processing Systems (NeurIPS)*, 2016.
- [25] C. E. Rasmussen and C. K. I. Williams. *Gaussian Processes for Machine Learning*. MIT Press, 2006.
- [26] S. E. Reed, H. Lee, D. Anguelov, C. Szegedy, D. Erhan, and A. Rabinovich. Training deep neural networks on noisy labels with bootstrapping. In *International Conference on Learning Representations (ICLR)*, 2015.
- [27] G. Singh, J. Yoon, Y. Son, and S. Ahn. Sequential neural processes. In *Neural Information Processing Systems (NeurIPS)*, 2019.

- [28] A. Vaswani, N. Shazeer, N. Parmar, J. Uszkoreit, L. Jones, A. N. Gomez, L. Kaiser, and I. Polosukhin. Attention is all you need. In *Neural Information Processing Systems (NeurIPS)*, 2017.
- [29] D. J. Wilkinson. *Stochastic modelling for systems biology*. CRC Press, 2011.
- [30] T. Willi, J. Masci, J. Schmidhuber, and C. Osendorfer. Recurrent neural processes. *arXiv preprint arXiv:1906.05915*, 2019.
- [31] M. Zaheer, S. Kottur, S. Ravanbakhsh, B. Póczos, R. Salakhutdinov, and A. Smola. Deep sets. In *Neural Information Processing Systems (NeurIPS)*, 2017.

Appendices

A Model Architectures

A.1 CNP, NP and BNP

We borrowed most of the architectures from the paper [15] and their source code released ³.

Encoder Let $\text{MLP}(\ell, d_{\text{in}}, d_h, d_{\text{out}})$, ($\ell \geq 2$) be a multilayer perceptron having the structure

$$\begin{aligned} \text{MLP}(\ell, d_{\text{in}}, d_h, d_{\text{out}}) &= \text{Linear}(d_h, d_{\text{out}}) \\ &\quad \circ \underbrace{(\text{ReLU} \circ \text{Linear}(d_h, d_h) \circ \dots)}_{\times(\ell-2)} \\ &\quad \circ \text{Linear}(d_h, d_{\text{in}}). \end{aligned} \tag{A.1}$$

An encoder of a NP consists of a deterministic path and a latent path using two identical structures (but with separate parameters),

$$\begin{aligned} h_1 &= \frac{1}{|c|} \sum_{i \in c} \text{MLP}(\ell_{\text{pre}}, d_x + d_y, d_h, d_h)([x_i, y_i]), \\ \phi &= \text{MLP}(\ell_{\text{post}}, d_h, d_h)(h_1), \quad f_{\text{denc}}(X_c, Y_c) = \phi \\ h_2 &= \frac{1}{|c|} \sum_{i \in c} \text{MLP}(\ell_{\text{pre}}, d_x + d_y, d_h, d_h)([x_i, y_i]), \\ (\eta, \rho') &= \text{MLP}(\ell_{\text{post}}, d_h, 2d_z)(h_2), \\ \rho' &= 0.1 + 0.9 \cdot \text{sigmoid}(\tilde{\rho}), \quad f_{\text{enc}}(X_c, Y_c) = (\eta, \rho), \end{aligned} \tag{A.2}$$

where d_x and d_y are the dimensionalities of x and y respectively, and d_h is fixed to 128 for all experiments.

An original CNP uses only one deterministic encoder, but that would perform worse than NP because it uses twice less number of parameters. For a fair comparison, we used two identical encoders for CNP as well.

$$\begin{aligned} h_1 &= \frac{1}{|c|} \sum_{i \in c} \text{MLP}(\ell_{\text{pre}}, d_x + d_y, d_h, d_h)([x_i, y_i]), \\ \phi_1 &= \text{MLP}(\ell_{\text{post}}, d_h, d_h)(h_1) \\ h_2 &= \frac{1}{|c|} \sum_{i \in c} \text{MLP}(\ell_{\text{pre}}, d_x + d_y, d_h, d_h)([x_i, y_i]), \\ \phi_2 &= \text{MLP}(\ell_{\text{post}}, d_h, d_h)(h_2) \\ \phi &= [\phi_1, \phi_2], \quad f_{\text{enc}}(X_c, Y_c) = \phi. \end{aligned} \tag{A.3}$$

BNP uses exactly the same network encoder as CNP.

Decoder A decoder in CNP and NP take a representation of a context and transform it to parameters of conditional probability. Let x_* be a target data point. A decoder of CNP is defined as

$$\begin{aligned} (\mu, \sigma') &= \text{MLP}(\ell_{\text{dec}}, 2d_h + d_x, d_h, 2d_y)([\phi, x_*]) \\ \sigma &= 0.1 + 0.9 \cdot \text{softplus}(\sigma'), \quad f_{\text{dec}}(\phi, x_*) = (\mu, \sigma). \end{aligned} \tag{A.4}$$

A decoder for NP uses exactly the same architecture except for that it takes $[\phi, z]$ instead.

$$\begin{aligned} (\mu, \sigma') &= \text{MLP}(\ell_{\text{dec}}, d_h + d_z + d_x, d_h, 2d_y)([\phi, z, x_*]) \\ \sigma &= 0.1 + 0.9 \cdot \text{softplus}(\sigma'), \quad f_{\text{dec}}(\phi, x_*) = (\mu, \sigma). \end{aligned} \tag{A.5}$$

³<https://github.com/deepmind/neural-processes>

BNP uses the same decoder as CNP when computing the deterministic representation without bootstrapping (base model). When decoding an aggregated representations from an original context ϕ and a bootstrapped context $\tilde{\phi}$, we add an adaptation layer to the first linear layer of the MLP.

$$\begin{aligned}
h_1 &= \text{Linear}(2d_h + d_x, d_h)([\phi, x_*]) \\
h_2 &= \text{Linear}(2d_h, d_h)(\tilde{\phi}) \quad (\text{adaptation layer}) \\
(\mu, \sigma') &= \text{MLP}(\ell_{\text{dec}} - 1, d_h, d_h, 2d_y)(\text{ReLU}(h_1 + h_2)) \\
\sigma &= 0.1 + 0.9 \cdot \text{softplus}(\sigma'), \quad f_{\text{dec}}(\phi, \tilde{\phi}, x_*) = (\mu, \sigma).
\end{aligned} \tag{A.6}$$

A.2 CANP, ANP and BANP

Encoder An encoder of ANP has a deterministic path and latent path. A deterministic path uses a self-attention and cross-attention to summarize contexts. Let $\text{MHA}(d_{\text{out}})$ be a multi-head attention [28] computed as follows:

$$\begin{aligned}
Q' &= \{\text{Linear}(d_q, d_{\text{out}})(q)\}_{q \in Q}, \quad \{Q'_j\}_{j=1}^{n_{\text{head}}} = \text{split}(Q', n_{\text{head}}) \\
K' &= \{\text{Linear}(d_k, d_{\text{out}})(k)\}_{k \in K}, \quad \{K'_j\}_{j=1}^{n_{\text{head}}} = \text{split}(K', n_{\text{head}}) \\
V' &= \{\text{Linear}(d_v, d_{\text{out}})(v)\}_{v \in V}, \quad \{V'_j\}_{j=1}^{n_{\text{head}}} = \text{split}(V', n_{\text{head}}) \\
H_j &= \text{softmax}(Q'_j(K'_j)^\top / \sqrt{d_{\text{out}}})V'_j, \quad H = \text{concat}(\{H_j\}_{j=1}^{n_{\text{head}}}) \\
H' &= \text{LN}(Q' + H) \\
\text{MHA}(d_{\text{out}})(Q, K, V) &= \text{LN}(H' + \text{ReLU}(\text{Linear}(d_{\text{out}}, d_{\text{out}}))).
\end{aligned} \tag{A.7}$$

Here, (q_k, q_k, q_v) denotes the dimensionalities of query Q , key K , and value V respectively, d_{out} is an output dimension, n_{head} is a number of heads, split and concat are splitting and concatenating operation in feature axis, and LN is the layer normalization [1]. A self-attention is defined as simply tying $Q = K = V$, $\text{SA}(d_{\text{out}})(X) = \text{MHA}(d_{\text{out}})(X, X, X)$. A deterministic path of ANP is then defined as

$$\begin{aligned}
f_{\text{qk}} &= \text{MLP}(\ell_{\text{qk}}, d_x, d_h, d_h) \\
q &= f_{\text{qk}}(x_*), \quad K = \{f_{\text{qk}}(x_i)\}_{i \in c} \\
V &= \text{SA}(d_h)(\{\text{MLP}(\ell_v, d_x + d_y, d_h)([x_i, y_i])\}_{i \in c}) \\
\phi &= \text{MHA}(d_h)(q, K, V), \quad f_{\text{dec}}(X_c, Y_c, x_*) = \phi.
\end{aligned} \tag{A.8}$$

A latent path of ANP is

$$\begin{aligned}
H &= \text{SA}(d_h)(\{\text{ReLU} \circ \text{MLP}(\ell_{\text{pre}}, d_x + d_y, d_h, d_h)([x_i, y_i])\}_{i \in c}) \\
(\eta, \rho') &= \text{MLP}(\ell_{\text{post}}, d_h, 2d_z) \left(\frac{1}{|c|} \sum_{i \in c} h_i \right) \\
\rho &= 0.1 + 0.9 \cdot \text{sigmoid}(\rho'), \quad (\eta, \rho) = f_{\text{enc}}(X_c, Y_c).
\end{aligned} \tag{A.9}$$

For CANP and BANP, we use the same architecture having two paths as follows:

$$\begin{aligned}
f_{\text{qk}} &= \text{MLP}(\ell_{\text{qk}}, d_x, d_h, d_h) \\
q &= f_{\text{qk}}(x_*), \quad K = \{f_{\text{qk}}(x_i)\}_{i \in c} \\
V &= \text{SA}(d_h)(\{\text{MLP}(\ell_v, d_x + d_y, d_h)([x_i, y_i])\}_{i \in c}) \\
\phi_1 &= \text{MHA}(d_h)(q, K, V) \\
H &= \text{SA}(d_h)(\{\text{ReLU} \circ \text{MLP}(\ell_{\text{pre}}, d_x + d_y, d_h, d_h)([x_i, y_i])\}_{i \in c}) \\
\phi_2 &= \text{MLP}(\ell_{\text{post}}, d_h, d_h) \left(\frac{1}{|c|} \sum_{i \in c} h_i \right) \\
\phi &= [\phi_1, \phi_2], \quad f_{\text{enc}}(X_c, Y_c, x_*) = \phi.
\end{aligned} \tag{A.10}$$

Decoder Decoders are the same is in [Appendix A.1](#).

B Experimental Details

B.1 1D Regression

Architectures For models without attention (CNP, NP, BNP), we set $\ell_{\text{pre}} = 4, \ell_{\text{post}} = 2, \ell_{\text{dec}} = 3, d_h = 128$. For NP we set $d_z = 128$. For models with attention (CANP, ANP, BANP), we set $\ell_v = 2, \ell_{\text{qk}} = 2, \ell_{\text{pre}} = 2, \ell_{\text{post}} = 2, \ell_{\text{dec}} = 3, d_h = 128, n_{\text{head}} = 8$ and $d_z = 128$ for ANP.

Data generation We trained all the models using data generated from GPs with RBF kernel. For each task (X, Y, c) , we first generated $x \stackrel{\text{i.i.d.}}{\sim} \text{Unif}(-2, 2)$ and generated Y from using RBF Kernel $k(x, x') = s^2 \cdot \exp(-\|x - x'\|^2 / 2\ell^2)$ with $s \sim \text{Unif}(0.1, 1.0)$ and $\ell \sim \text{Unif}(0.1, 0.6)$, and output additive noise $\mathcal{N}(0, 10^{-2})$. The size of the task and the size of the context c was drawn as $|c| \sim \text{Unif}(3, 47)$ and $n - |c| \sim \text{Unif}(3, 50 - |c|)$. For model-data mismatch scenario, we generated data from GP with Matern52 kernels, periodic kernels, and GP with RBF kernel plus Student’s t noise. For Matern52 kernel $k(x, x') = s^2(1 + \sqrt{5}d/\ell + 5d^2/(3\ell^2)) \exp(-\sqrt{5}d/\ell)$, ($d = \|x - x'\|$), we sampled $s \sim \text{Unif}(0.1, 1.0)$ and $\ell \sim \text{Unif}(0.1, 0.6)$. For periodic kernel $k(x, x') = s^2 \exp(-2 \sin^2(\pi\|x - x'\|^2/p)/\ell^2)$, we sampled $s \sim \text{Unif}(0.1, 1.0)$ and $\ell \sim \text{Unif}(0.1, 0.6)$ and $p \sim \text{Unif}(0.1, 0.5)$. For Student- t noise, we added $\varepsilon \sim \gamma \cdot \mathcal{T}(2.1)$ to the curves generated from GP with RBF kernel, where $\mathcal{T}(2.1)$ is a Student’s t distribution with degree of freedom 2.1 and $\gamma \sim \text{Unif}(0, 0.15)$.

Training and testing We trained all the model for 100,000 steps with each step computes updates with a batch containing 100 tasks. We used Adam optimizer [17] with initial learning rate $5 \cdot 10^{-4}$ and decayed the learning rate using cosine annealing scheme. NP and ANP were trained using $k = 4$ samples for z (as in [4]), and tested with $k = 50$ samples. BNP and BANP were trained with $k = 4$ bootstrap contexts and tested with $k = 50$ samples. The size of the task and the size of the context c was drawn as $|c| \sim \text{Unif}(3, 200)$ and $n - |c| \sim \text{Unif}(3, 200 - |c|)$. Testings were done for 3,000 batches with each batch containing 16 tasks (48,000 tasks in total).

B.2 Bayesian Optimization

Architectures / Training and testing For these experiments, we followed the settings described in Section 5.1.

Prior function generation We sampled 100 GP prior functions from zero mean and unit variance. After realizing them, the prior functions are used to optimize via Bayesian optimization. We normalized these functions in order to fairly compare simple regrets and cumulative regrets across distinct sampled functions (Basically, since they are sampled from same distributions, the scales of them are quite similar, but we used more precise evaluations).

Bayesian optimization setting As presented in the Bayesian optimization results, all the methods are started from same initializations. We employed Gaussian process regression [25] with squared exponential kernels as a surrogate model, and expected improvement [14] as an acquisition function, which is optimized by the multi-started local optimization method, L-BFGS-B with 100 initial points. All the experiments are implemented with [16].

B.3 Image Completion

EMNIST architectures For models without attention (CNP, NP, BNP), we set $\ell_{\text{pre}} = 5, \ell_{\text{post}} = 3, \ell_{\text{dec}} = 4, d_h = 128$. For NP we set $d_z = 128$. For models with attention (CANP, ANP, BANP), we set $\ell_v = 3, \ell_{\text{qk}} = 3, \ell_{\text{pre}} = 3, \ell_{\text{post}} = 3, \ell_{\text{dec}} = 4, d_h = 128, n_{\text{head}} = 8$ and $d_z = 128$ for ANP.

CelebA32 architectures For models without attention (CNP, NP, BNP), we set $\ell_{\text{pre}} = 6, \ell_{\text{post}} = 3, \ell_{\text{dec}} = 5, d_h = 128$. For NP we set $d_z = 128$. For models with attention (CANP, ANP, BANP), we set $\ell_v = 4, \ell_{\text{qk}} = 3, \ell_{\text{pre}} = 4, \ell_{\text{post}} = 3, \ell_{\text{dec}} = 5, d_h = 128, n_{\text{head}} = 8$ and $d_z = 128$ for ANP.

Data generation Each task (X, Y, c) was sampled from an image. Following [10, 15], we sampled 2D coordinates from an image and rescaled the values into $[-1, 1]$ to comprise X , and rescaled the

Table C.1: Calibration error and sharpness of the models for 1D regression experiments. Means and standard deviations of 5 runs are reported.

	RBF		Matérn 5/2		Periodic		t -noise	
	CE	Sharpness	CE	Sharpness	CE	Sharpness	CE	Sharpness
CNP	0.059±0.003	0.072±0.001	0.012±0.001	0.079±0.001	0.171±0.004	0.226±0.004	0.029±0.002	0.093±0.001
NP	0.016±0.001	0.06±0.001	0.037±0.005	0.067±0.001	0.306±0.016	0.224±0.001	0.138±0.012	0.082±0.001
BNP	0.049±0.002	0.069±0.000	0.011±0.001	0.077±0.000	0.145±0.002	0.243±0.008	0.032±0.001	0.098±0.001
CANP	0.276±0.005	0.057±0.001	0.127±0.003	0.066±0.000	0.251±0.022	0.157±0.006	0.038±0.003	0.086±0.002
ANP	0.144±0.009	0.048±0.001	0.051±0.003	0.055±0.002	0.402±0.031	0.165±0.007	0.154±0.014	0.074±0.003
BANP	0.264±0.001	0.057±0.000	0.121±0.001	0.067±0.000	0.0.226±0.002	0.176±0.003	0.035±0.001	0.095±0.001

corresponding pixel values into $[-0.5, 0, 5]$ to comprise Y . The size of the task and the size of the context c was drawn as $|c| \sim \text{Unif}(3, 200)$ and $n - |c| \sim \text{Unif}(3, 200 - |c|)$. For EMNIST we used the first 10 classes during training, and tested on remaining 37 classes as a model-data mismatch scenario.

Training and testing Same as Section 5.1, except that all the models were trained for 200 epochs through the datasets. The models were tested on entire test set where each sample in a test set comprises a task. For a model-data mismatch scenario with Student’s t noise, we added $\varepsilon \sim \gamma \cdot \mathcal{T}(2.1)$ with $\gamma \sim \text{Unif}(0, 0.09)$ to Y .

B.4 Lotka-Volterra

Architectures For models without attention (CNP, NP, BNP), we set $\ell_{\text{pre}} = 4, \ell_{\text{post}} = 2, \ell_{\text{dec}} = 3, d_h = 128$. For NP we set $d_z = 128$. For models with attention (CANP, ANP, BANP), we set $\ell_{\text{pre}} = 2, \ell_{\text{post}} = 2, \ell_{\text{dec}} = 3, d_h = 128, n_{\text{head}} = 8$ and $d_z = 128$ for ANP.

Dataset generation We followed the setting in [11], please refer to the description in the paper. A task (X, Y, c) is then constructed by uniformly subsampling X and corresponding Y from the generated series. The size of the task and the size of the context c was drawn as $|c| \sim \text{Unif}(15, 85)$ and $n - |c| \sim \text{Unif}(15, 100 - |c|)$. Due to the scaling issue, X and Y values were standardized using the statistics computed from the context:

$$x'_i = \frac{x_i - \text{mean}(X_c)}{\text{std}(X_c) + 10^{-5}}, \quad y'_i = \frac{y_i - \text{mean}(Y_c)}{\text{std}(Y_c) + 10^{-5}}. \quad (\text{B.11})$$

Training and testing We trained for 100,000 steps with each step is computed with a batch containing 50 tasks. The other details are the same as in Section 5.1. Testing was done on 3,000 batches with each batch containing 16 tasks. For real-data testing as a model-data mismatch scenario, following [11], we generated 1,000 batches with each batch containing 16 tasks from Hudson’s Bay hare-lynx data. Each task contained $|c| \sim \text{Unif}(15, 76)$ and $n \sim \text{Unif}(15, 91 - |c|)$ points subsampled from the data, and standardized as above.

C On calibration and sharpness of the models

We further analyze the learned models using the framework introduced in [18]. Let $\mathcal{T} = (X, Y, c)$ be a task. We see how the predictions for the targets $\{(x_i, y_i)\}_{i \notin c}$ is calibrated, and how large the variances are. Let $F_{x_i}(y_i)$ be the CDF of the prediction $p(y_i | x_i, X_c, Y_c)$. We say a model is perfectly calibrated [18] if for any $p \in [0, 1]$,

$$\frac{1}{n - |c|} \sum_{i \notin c} \mathbb{1}_{\{y_i \leq F_{x_i}^{-1}(p)\}} \rightarrow p \text{ as } n \rightarrow \infty, \quad (\text{C.12})$$

The calibration error (CE) is then defined as

$$0 \leq p_1 \leq \dots \leq p_m \leq 1, \quad \hat{p}_\ell = \frac{1}{n - |c|} \sum_{i \notin c} \mathbb{1}_{\{y_i \leq F_{x_i}^{-1}(p_\ell)\}}, \quad \text{CE}(\mathcal{T}) = \sum_{\ell=1}^m (p_\ell - \hat{p}_\ell)^2. \quad (\text{C.13})$$

Table C.2: Calibration error and sharpness of the models for EMNIST experiments. Means and standard deviations of 5 runs are reported.

	Seen classes (0-9)		Unseen classes (10-46)		t -noise	
	CE	sharpness	CE	Sharpness	CE	Sharpness
CNP	0.448±0.007	0.035±0.001	0.355±0.007	0.043±0.001	0.066±0.008	0.066±0.055
NP	0.423±0.007	0.042±0.001	0.337±0.004	0.050±0.001	0.046±0.008	0.069±0.001
BNP	0.435±0.007	0.037±0.001	0.342±0.006	0.046±0.001	0.044±0.014	0.070±0.003
CANP	0.533±0.006	0.029±0.000	0.463±0.003	0.032±0.000	0.327±0.065	0.085±0.006
ANP	0.489±0.010	0.034±0.001	0.442±0.008	0.036±0.001	0.197±0.041	0.085±0.006
BANP	0.511±0.011	0.032±0.001	0.449±0.006	0.035±0.001	0.117±0.023	0.076±0.006

Table C.3: Calibration error and sharpness of the models on CelebA32 experiments. Means and standard deviations of 5 runs are reported.

	Without noise		t -noise	
	CE	Sharpness	CE	Sharpness
CNP	0.019±0.000	0.056±0.000	0.003±0.000	0.080±0.002
NP	0.017±0.000	0.065±0.000	0.062±0.002	0.009±0.003
BNP	0.008±0.000	0.065±0.009	0.035±0.006	0.101±0.002
CANP	0.069±0.000	0.054±0.000	0.007±0.002	0.110±0.010
ANP	0.018±0.000	0.062±0.000	0.082±0.002	0.096±0.001
BANP	0.018±0.000	0.065±0.000	0.075±0.012	0.100±0.002

In our case, we set $p(y_i|x_i, X_c, Y_c) = \mathcal{N}(y_i|\mu_i, \sigma_i^2)$, so

$$F_{x_i}^{-1}(p_\ell) = \mu_i + \sigma_i \sqrt{2} \operatorname{erf}^{-1}(2p_\ell - 1). \quad (\text{C.14})$$

For the models using the ensemble of multiple predictions (NP, ANP, BNP, BANP), we report the ensembled calibration error.

$$(F_{x_i}^{(j)})^{-1}(p_\ell) = \mu_i^{(j)} + \sigma_i^{(j)} \sqrt{2} \operatorname{erf}^{-1}(2p_\ell - 1), \quad (\text{C.15})$$

$$\hat{p}_\ell^{(j)} = \frac{1}{n - |c|} \sum_{i \notin c} \mathbb{1}_{\{y_i \leq (F_{x_i}^{(j)})^{-1}(p_\ell)\}}, \quad (\text{C.16})$$

$$\text{CE}(\mathcal{T}) = \frac{1}{k} \sum_{j=1}^k \sum_{i=1}^n (p_\ell - \hat{p}_\ell^{(j)})^2. \quad (\text{C.17})$$

We also measure the sharpness [18] which essentially is a average prediction variance.

$$\text{Sharpness}(\mathcal{T}) = \frac{1}{n - |c|} \sum_{i \notin c} \sigma_i^2. \quad (\text{C.18})$$

We evaluated the CE and sharpness of CNP, NP, BNP, CANP, ANP, and BANP trained in the experiments. The results are summarized in Tables C.1 to C.4. In general, ours (BNP and BANP) were better

Table C.4: Calibration error and sharpness of the models on Predator-prey experiments. Means and standard deviations of 5 runs are reported.

	Simulated		Real	
	CE	Sharpness	CE	Sharpness
CNP	0.001±0.000	0.578±0.013	0.072±0.008	1.866±0.058
NP	0.002±0.003	0.567±0.009	0.087±0.000	1.877±0.069
BNP	0.003±0.000	0.542±0.016	0.076±0.011	1.975±0.004
CANP	0.146±0.003	0.076±0.001	0.565±0.034	0.350±0.034
ANP	0.104±0.004	0.064±0.001	0.814±0.036	0.248±0.015
BANP	0.140±0.003	0.074±0.001	0.539±0.039	0.352±0.019

Table D.5: Ablation study for 1D regression.

	RBF		Matérn 5/2		Periodic		t -noise	
	context	target	context	target	context	target	context	target
BNP	1.012±0.006	0.523±0.004	0.891±0.007	0.316±0.004	-0.111±0.002	-1.089±0.009	0.554±0.006	-0.644±0.010
naïve bootstrap	0.774±0.015	0.304±0.011	0.642±0.017	0.088±0.008	-0.261±0.004	-1.368±0.019	0.329±0.012	-1.203±0.030
- paired bootstrap	0.990±0.005	0.491±0.004	0.865±0.006	0.269±0.004	-0.144±0.004	-1.342±0.014	0.455±0.037	-1.130±0.025
- adaptation layer	0.900±0.010	0.455±0.007	0.803±0.011	0.294±0.006	0.009±0.008	-0.845±0.006	0.579±0.010	-0.337±0.015
- p_{base} loss	0.992±0.010	0.496±0.007	0.868±0.011	0.273±0.007	-0.135±0.010	-1.315±0.016	0.468±0.014	-1.068±0.032
BNP	1.379±0.000	0.849±0.001	1.376±0.000	0.671±0.001	0.688±0.044	-3.429±0.084	1.137±0.007	-1.750±0.031
naïve bootstrap	1.365±0.008	0.822±0.014	1.356±0.011	0.632±0.014	0.502±0.068	-3.729±0.151	1.041±0.023	-1.782±0.020
- paired bootstrap	1.379±0.000	0.841±0.002	1.377±0.000	0.655±0.002	0.830±0.031	-4.510±0.138	1.141±0.014	-2.179±0.019
- adaptation layer	1.370±0.000	0.830±0.001	1.361±0.000	0.639±0.002	0.523±0.030	-3.598±0.099	1.046±0.003	-1.765±0.014
- p_{base} loss	1.378±0.000	0.836±0.002	1.375±0.000	0.661±0.001	0.647±0.041	-3.801±0.294	1.132±0.004	-1.697±0.050

calibrated for model-data mismatch settings, but worse calibrated than NP and ANP for normal test settings or model-data mismatch settings not very different from the normal test setting (e.g., Matérn 5/2 kernels in 1D regression experiments and unseen classes for EMNIST). The reason is that, as we stated in the main text, BNP and BANP tends to produce conservative credible intervals, so become under-confident in normal-test settings and less over-confident in mismatch settings. This corresponds to the observation and theory in [13], where BayesBag is proven to yield credible intervals that are twice larger than the credible intervals produced by normal Bayesian models when the model is correctly specified. The sharpness values also support this claim, where BNP and BANP generally shows higher values than others especially for the mismatch settings. Interestingly, CNP and CANP exhibit similar trends to ours (larger sharpness values than NP or ANP), presumably because they output only one predictor without any functional uncertainty and thus are encouraged to be conservative than NP or ANP to cover wider range predictions. Still, BNP and BANP produced the largest sharpness values in overall. Although this trend we discussed is apparent in 1D regression and predator-prey experiments, we fail to find any of such trend for image completion experiments. We conjecture that this is because for image completion experiments we are restricting the range of function values y to lie in $[-0.5, 0.5]$. This suggests that at least for image completion experiments, the robustness of ours (which is clearly demonstrated both in terms of likelihood values and qualitative samples) comes from a different reason.

D Additional results

D.1 1D Regression

Ablation study We present an ablation study to empirically validate our design choices for BNP and BANP on 1D regression experiment. We compared our full model to the followings: 1) naïve residual bootstrap applied to CNP and CANP as described in Section 3.1, 2) BNP and BANP without context resampling via paired bootstrap, and 3) BNP and BANP without adaptation path so decoder just taking the representations of bootstrapped contexts, and 4) BNP and BANP trained without additional p_{base} loss in Eq. (14). Table D.5 summarizes the results. Except for the case without adaptation layer which showed slightly better performance on mismatch settings, every ablation cases showed poor performance. Naïve bootstrap didn’t work well for both normal test and mismatch settings, the models without paired bootstrap worked poorly on mismatch settings, and the models without adaptation layer didn’t perform well on normal test settings.

Training time We measured averaging training time per batch for CNP, NP, and BNP on 1D regression task (Fig. D.1, left). BNP forwards the data to the model twice, but the actual computation time for BNP is less than the twice of the computation time of NP, because the first pass to compute residuals uses only the context set (X_c, Y_c) which is a subset of the entire batch (X, Y) . Thanks to the parallelization by packing every dataset into a tensor, the computation times for all models does not scale linearly with the number of samples k .

Performance for various dataset size n We measured the average target log-likelihood with varying dataset size n on 1D regression task (Fig. D.1, right). BNP uniformly performed better than CNP and NP by a significant margin.

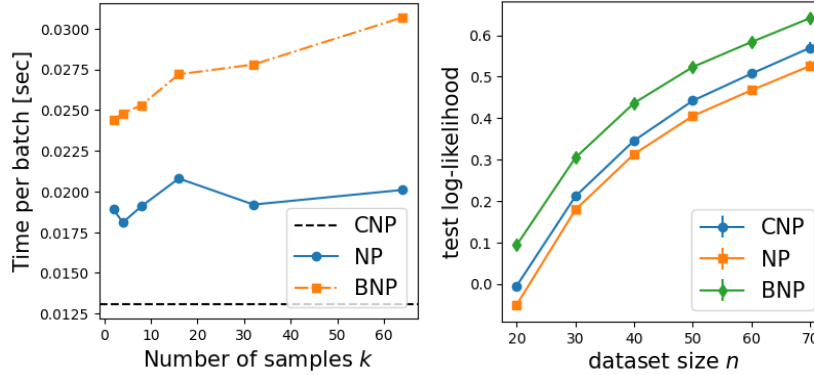


Figure D.1: (Left) processing time per batch. (Right) log-likelihood with different dataset sizes n .

Additional figures Here we present additional samples in [Fig. D.2](#).

D.2 Bayesian optimization

Bayesian optimization results, showed in [Fig. D.3](#) demonstrate our methods outperform or are comparable to other methods including GP oracle. For the RBF case, GP oracle is the best result, but our models show the second best results and become comparable to the GP oracle at the last of iterations. On the contrary, in the model-data mismatch setting with t -noise (see the second row of [Fig. D.3](#)), our methods outperform other methods, which implies that our methods, BNP and BANP are robust to the heavy-tailed noises. Moreover, while CNP and CANP models show the better results in Matérn 5/2 and Periodic cases, our methods are comparable to those methods, as shown in the last two rows of [Fig. D.3](#).

D.3 Image completion

We present additional visualizations for EMNIST in [Fig. D.4](#) and for CelebA in [Fig. D.5](#).

D.4 Predator-prey model

We present additional visualizations for predator-prey experiment in [Fig. D.6](#).

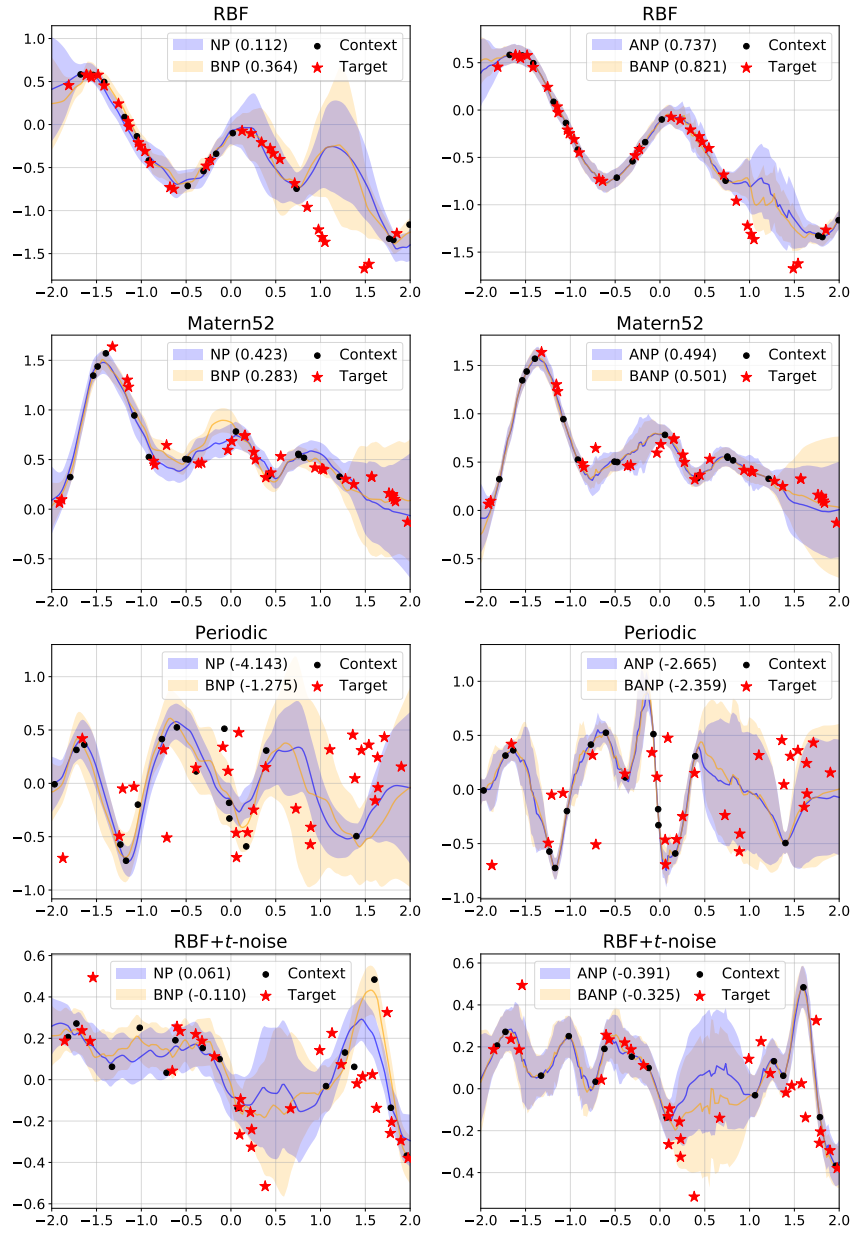


Figure D.2: More visualizations for 1D regression experiment.

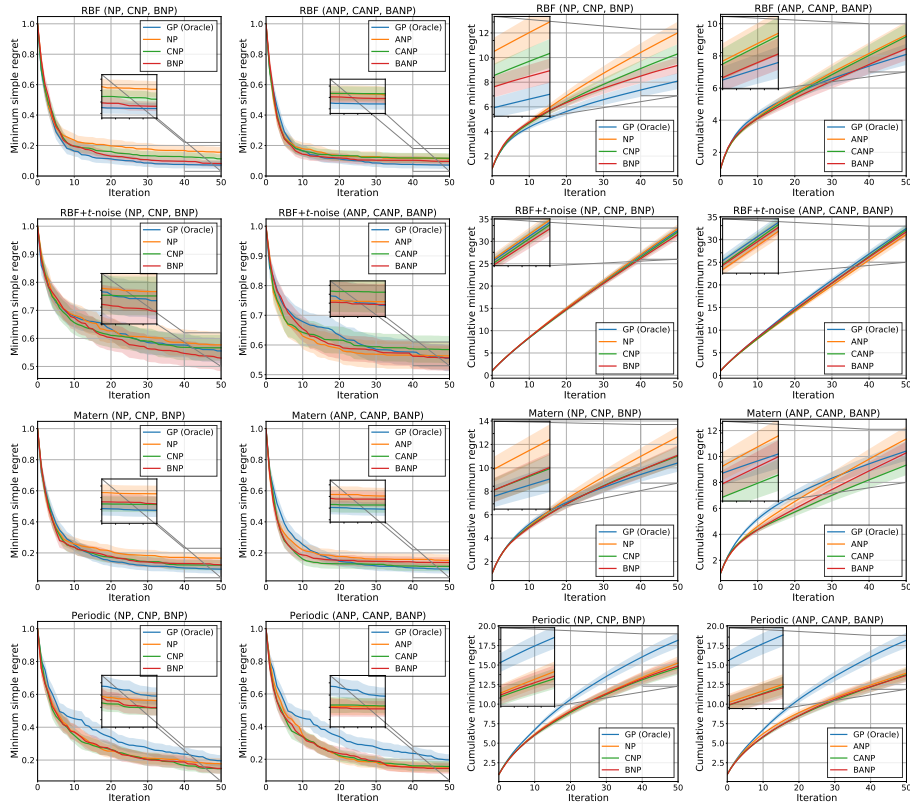


Figure D.3: Bayesian optimization results for GP prior functions with (first row) RBF kernel, (second row) RBF kernel + t -noise, (third row) Matern 5/2 kernel, and (fourth row) Periodic kernel.

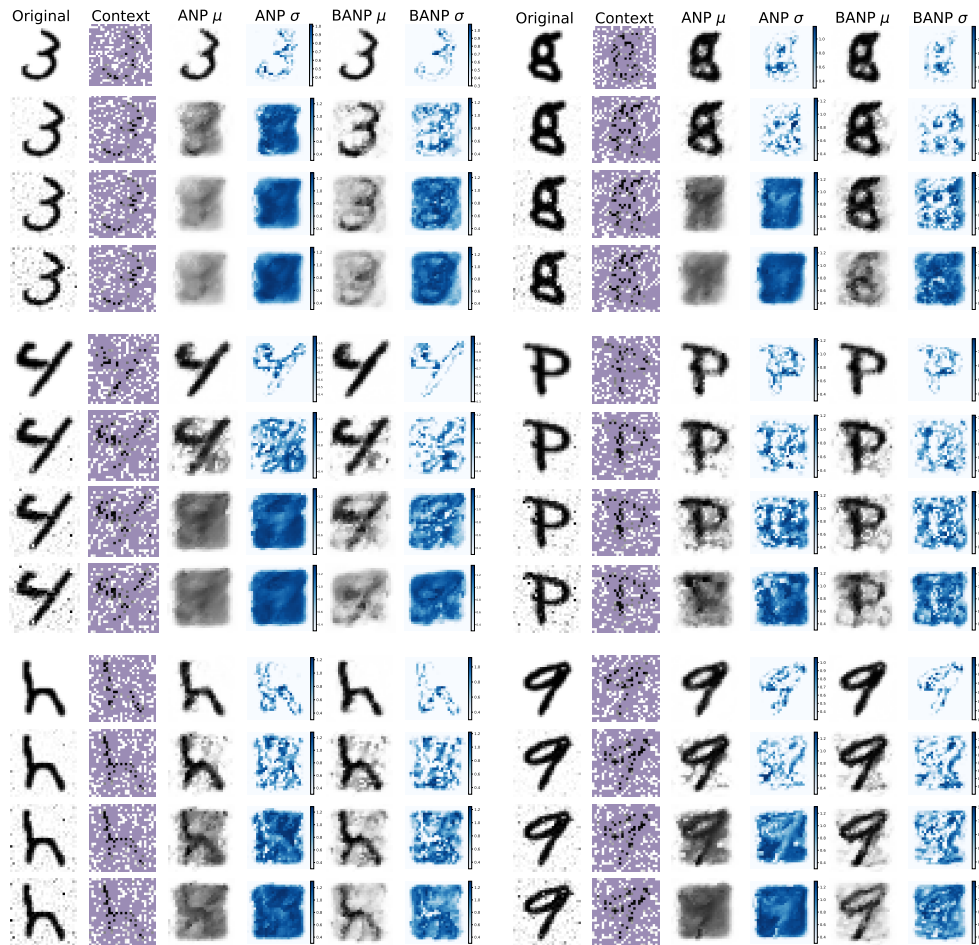


Figure D.4: Image completion results on EMNIST for ANP and BANP. The results under increasing noise levels are shown.



Figure D.5: Image completion results on CelebA32 for ANP and BANP. The results under increasing noise levels are shown.

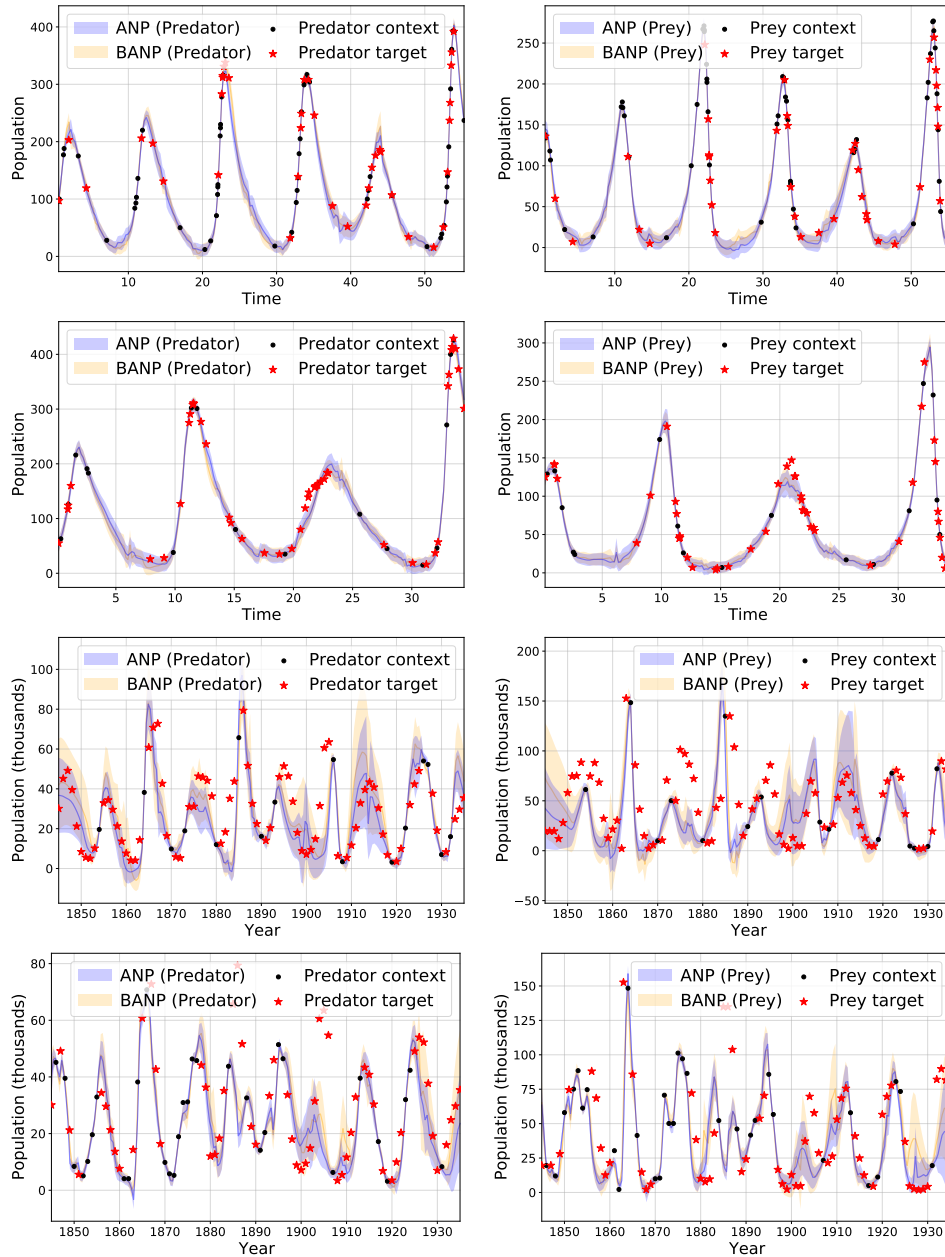


Figure D.6: Regression results for predator-prey data. First two rows shows the results for simulated data, and the last two rows shows the results for the real data (Hudson's Bay hare-lynx data).